Materials Today Bio 31 (2025) 101469

Contents lists available at ScienceDirect

Materials Today Bio

journal homepage: www.journals.elsevier.com/materials-today-bio

Sustained release of miR-21 carried by mesenchymal stem cell-derived exosomes from GelMA microspheres inhibits ovarian granulosa cell apoptosis in premature ovarian insufficiency

Xiaofei Zhang [1], Linzi Ma [1], Xiaotong Liu [1], Xingyu Zhou, Ao Wang, Yunhui Lai, Jun Zhang, Ying Li, Shiling Chen [*]

Center for Reproductive Medicine, Department of Gynecology and Obstetrics, Nanfang Hospital, Southern Medical University, Guangzhou, 510515, China

ARTICLE INFO

Keywords:
Exosomes
Mesenchymal stem cell
GelMA hydrogel
Ovarian granulosa cells
Premature ovarian insufficiency

ABSTRACT

Background: Premature ovarian insufficiency (POI) refers to the severe decline or failure of ovarian function in women younger than 40 years of age. It is a serious hazard to women's physical and mental health, but current treatment options are limited. Mesenchymal stem cell-derived exosomes (MSC-Exo) exhibit promising potential as a therapeutic approach for POI. However, their clinical application is hindered by their instability and low long-term retention rate *in vivo*.

Methods and results: In this study, miR-21 was identified as the predominant miRNA with low-expression in follicular fluid exosomes of POI patients and was shown to possess antiapoptotic activity. Next, we loaded miR-21 agomir to MSC-Exo to form Agomir21-Exo, which significantly reversed the apoptosis of granulosa cells *in vitro*. Moreover, we successfully developed GelMA hydrogel microspheres for encapsulating Agomir21-Exo through microfluidic technology, named GelMA-Ag21Exo, which had good injectability and significantly enhanced the stability and long-term retention of Agomir21-Exo in mice through sustained release. The release of Agomir21-Exo from GelMA-Ag21Exo notably alleviated the apoptosis of ovarian granulosa cells and improved the ovarian reserve and fertility in POI mice.

Conclusion: Our findings illustrate that activating miR-21 through Agomir21-Exo could improve the function of ovarian granulosa cells. The GelMA-Ag21Exo enhanced the exosome-based therapeutic efficacy of the Agomir21-Exo *in vivo*. These findings provide a novel and promising treatment strategy for POI patients.

1. Introduction

Premature ovarian insufficiency (POI) refers to the loss of ovarian function in women under the age of 40. It is primarily characterized by amenorrhea, follicle-stimulating hormone (FSH) level exceeding 25 IU/L, reduced estrogen level, varying degrees of perimenopausal symptoms and infertility [1,2]. The terminal stage of this disease is defined as premature ovarian failure (POF). At present, the main treatment for POI is hormone replacement therapy (HRT). However, HRT can only alleviate perimenopausal symptoms, and cannot truly restore the endocrine function of the ovaries [3].

In mammals, ovarian granulosa cell (GC) dysfunction can lead to follicular atresia and POI [4,5]. Both human and animal follicular fluid (FF) contain vast amounts of exosomes (FF-Exo), the primary carriers of microRNAs (miRNAs), which are generally thought to be closely related to the function of GCs [6–8]. Consequently, finding a miRNA from FF-Exo that can alleviate GC apoptosis may represent a natural and significant approach to the treatment of POI. However, it is common knowledge that the ovaries are located deep within the pelvic cavity, which makes local administration of medication difficult. Additionally, miRNAs are known to have low stability and are susceptible to degradation when unprotected in circulation.

Recently, numerous studies have reported the positive therapeutic effects of mesenchymal stem cells (MSCs) on the ovarian function of POI patients through various mechanisms, including improving homing, differentiation, and paracrine stimulation [9,10]. Recent research has

* Corresponding author. Center for Reproductive Medicine, Department of Gynecology and Obstetrics, Nanfang Hospital, Southern Medical University, 1838th North Guangzhou Avenue, Guangzhou, 510515, China.
E-mail address: chensl@smu.edu.cn (S. Chen).
[1] These authors contributed equally to this work.

https://doi.org/10.1016/j.mtbio.2025.101469
Received 18 April 2024; Received in revised form 4 January 2025; Accepted 7 January 2025
Available online 8 January 2025

attributed the regenerative potential of MSCs mainly to exosomes mediating paracrine effects [11,12]. On the one hand, mesenchymal stem cell-derived exosomes (MSC-Exo) can restore ovarian bioactivity and exhibit therapeutic effects similar to those of MSC transplantation [13]. On the other hand, MSC-Exo has great potential as a vector to deliver miRNAs to target cells because they are derived from allogeneic cells, so there is no need for safety concerns [14,15]. Therefore, we proposed a potential procedure for treating POI by integrating the miRNA into MSC-Exo, resulting in the formation of a miRNA-Exo complex with dual therapeutic effects.

However, the rapid metabolic rate and poor long-term retention of exosomes hinder the development of therapeutic methods based on MSC-Exo. Existing studies suggest that exosomes entering circulation are swiftly eliminated by the mononuclear phagocyte system (MPS), leading to insufficient accumulation of exosomes in target organs, thereby posing a significant hurdle for systemic exosome therapy [16]. Concurrently, under physiological conditions, small molecule drugs loaded in exosomes, such as miRNAs, will gradually lose their activity [17]. These issues prompted us to study the use of biomaterials that encapsulate MSC-Exo to optimize the application of MSC-Exo. Theoretically, encapsulation can enhance the stability and retention rate of MSC-Exo by providing protection and controlled sustained release.

In recent years, hydrogels have gained extensive attention in tissue engineering due to their superior biocompatibility and controllable drug delivery behavior [18,19]. However, due to their irregular shape, uncontrollable size and poor lubricity, ordinary hydrogels are prone to high and uneven injection forces during the injection process, resulting in tissue damage and patient discomfort. Given the stability and good flowability of spheres, cutting hydrogels into smaller hydrogel microspheres greatly enhances their injectability, benefiting *in vivo* applications [20–22]. Gelatin methacryloyl (GelMA) is a photopolymerizable hydrogel synthesized through the reaction of gelatin and methacrylic anhydride (MA) in phosphate-buffered saline. It is known for its controllable biodegradability, excellent biocompatibility, adjustable mechanical strength, and nontoxicity to the body [23]. The liquid GelMA hydrogel can transform into a stable solid-state under mild conditions (room temperature, neutral pH, etc.) through UV cross-linking [24]. This particular property makes it an ideal candidate for creating hydrogel microspheres using microfluidic technologies and has attracted increasing attention. The incorporation of different components to form composite hydrogels has been an effective strategy for improving certain characteristics of GelMA [23]. Studies have reported that after a low concentration of dimyristoylphosphatidylcholine (DMPC) lipids are added to the hydrogel for polymerization and cross-linking into composite hydrogels, the lipid boundary layer formed on the surface of the gel can significantly reduce the friction and wear of the hydrogel, enhancing its lubrication [25]. It is foreseeable that excellent lubrication is crucial for the injectability of hydrogel microspheres.

In this study, we designed GelMA hydrogel microspheres supplemented with DMPC (DMPC-GelMA). These microspheres were loaded with miRNA-Exo, allowing for smooth intra-abdominal injection. Furthermore, the microspheres controlled the release of miRNA-Exo *in vivo*, enhancing the bioavailability of miRNA-Exo and ultimately achieving therapeutic effects for POI.

2. Materials and methods

2.1. Patient samples and inclusion criteria

The study was conducted in accordance with the Declaration of Helsinki, and the protocol was approved by the Ethics Committee of Nanfang Hospital, Southern Medical University. Written informed consent was obtained from all patients. This study selected a subset of patients who were treated at the Reproductive Medicine Center of Nanfang Hospital from 2019 to 2022. The inclusion criteria for POI were as follows: (1) irregular menstrual cycle (<24 days or > 35 days) or amenorrhea for at least 4 months, and (2) an elevated FSH level ≥25 mIU/mL on two occasions ≥4 weeks apart. Patients with regular menstrual cycle who also met one of the following criteria at least were regarded as bPOI: (1) antral follicle count (AFC) ≤ 7; (2) anti-Müllerian hormone (AMH) ≤ 1.1 ng/mL; (3) 10 < basal FSH <25 mIU/mL [26,27]. The control group was women with severe male factor infertility or tubal/cervical factor infertility. Women in control group should have regular menstrual cycles (25–35 days), normal ovarian morphology and ovarian reserve (basal FSH <10 IU/mL, AFC >8, and AMH >1.1 ng/mL). The patients' ages were all below 40 years. Patients with gene mutations, iatrogenic ovarian damage, autoimmune diseases, and other reproductive endocrine diseases were excluded from our study.

2.2. Sample collection and preparation

For each patient who underwent *in vitro* fertilization (IVF) treatment with informed consent, FF was collected from only the first dominant follicle with a diameter exceeding 16–18 mm on the day of oocyte retrieval. Specifically, 2 mL of FF was aspirated from each chosen follicle. The collected FF was then centrifuged at 2000 rpm and 4 °C for 10 min. Immediately after this process, the samples were stored at −80 °C until exosome isolation.

Human granulosa cells (hGCs) were isolated from FF and subsequently digested at 37 °C for 10 min using 1–2 ml of Dulbecco's Modified Eagle's Medium (DMEM)/F-12 (HyClone, Logan, UT, USA) supplemented with 2 % hyaluronidase. The digested cells were collected by centrifugation at 1000 rpm for 5 min after digestion termination. The separated cells were inoculated in a 6-well plate for further cultivation.

2.3. Extraction and identification of FF-Exo

FF-Exo was extracted through ultracentrifugation. Briefly, FF was first centrifuged at 300×*g* for 10 min at 4 °C to remove cells. Subsequently, the cell debris was discarded through centrifugation at 2000×*g* for 20 min. This step was followed by additional centrifugation at 10,000×*g* for 30 min to eliminate apoptotic bodies and other biopolymers. The collected supernatant was then filtered through a 0.22 μm filter to remove particles larger than 200 nm. Further purification was performed on the Optima XPN-100 Ultracentrifuge (Beckman Coulter, Brea, CA, USA) at 4 °C with 120,000×*g* ultracentrifugation for 2 h. The resulting pellet was washed with PBS before being resuspended in PBS following another round of ultracentrifugation. The final exosome solution was either used immediately for experimentation or stored at −80 °C for future use.

According to the manufacturer's protocol, FF-Exo were resuspended and further diluted in 1 ml of PBS. Their concentration and particle size distribution were analysed using the Flow NanoAnalyzer U30E (NanoFCM, Xiamen, China). Particle morphology was observed using the HT-7700 transmission electron microscope (TEM) (Hitachi, Tokyo, Japan). Western blotting was utilized to detect the expression levels of exosomal markers (CD61, TSG101, and calnexin).

2.4. High-throughput sequencing of exosomal miRNAs

Library preparation and miRNA sequencing were conducted by Ribobio Company (Guangzhou, China). In brief, total RNA was extracted from FF-Exo, followed by reverse transcription of sRNA ranging between 18 and 30 nt into cDNA and subsequent amplification via PCR. The libraries that passed quality control were sequenced on the Illumina HiSeq 2500 platform. The specific sequencing data can be found in the Gene Expression Omnibus (GSE253684). Heatmap and Volcano plot were plotted by https://www.bioinformatics.com.cn (last accessed on Feb 20, 2024), an online platform for data analysis and visualization.

2.5. Exosomal RNA extraction and quantitative real-time PCR

According to the manufacturer's protocol, total RNA was extracted from FF-Exo using RNAiso Plus (Takara Bio, Japan). The first-strand cDNA was reverse transcribed using a PrimeScript RT Reagent Kit with gDNA Eraser (Takara), and quantitative real-time PCR (qRT-PCR) was performed using a SYBR Green PCR kit (Takara) on the ABI QuantStudio 5/6 (Thermo Fisher Scientific, MA, USA). Sequences of primers used to amplify miR-21, U6 are listed as follow: miR-21 forward 5′-GCGCGTAGCTTATCAGACTGA-3′, reverse 5′-TGGTGTTAAAGTC TTCTCAAATGC-3′; U6 forward 5′-CTCGCTTCGGCAGCACA-3′, reverse 5′-AACGCTTCACGAATTTGCGT-3′.

2.6. Cell culture and transfection

The immortalized human granulosa cell line KGN was acquired from the RIKEN BioResource Center (Tsukuba, Japan). The cells were cultured in Dulbecco's modified Eagle's medium (DMEM)/F-12 nutrient mixture supplemented with 10 % fetal bovine serum (Gibco, Life Technologies, Carlsbad, CA, USA) at 37 °C in a humidified incubator with 5 % CO2. miR-21-5p agomir/antagomir, NC agomir/antagomir were designed and synthesized by Ribobio company. KGN cells were transfected with Lipofectamine 3000 (Thermo Fisher Scientific, MA, USA).

2.7. Cell counting Kit-8 (CCK-8) assay

Cell proliferation was measured every 24 h using the CCK-8 assay kit (Dojindo Laboratories, Kumamoto, Japan). KGN cells were plated in a 96-well plate (3000 cells/well). Then, 10 μl of CCK-8 solution was added to each well 2 h before the absorbance measurement. The optical density was subsequently measured at 450 nm using spectrophotometry (Spectra Max M5). Each experiment was repeated three times, with five biological replicates each time.

2.8. Ethynyl-2-Deoxyuridine (EdU) assay

The EdU assay was performed according to the manufacturer's instructions (Ribobio). Briefly, cells were cultured in a 96-well plate (3000 cells/well) for 24 h followed by transfection, and 48 h post transfection, 50 μM EdU-labelled culture medium was added to each well, and continue incubating for 2 h. The medium was subsequently removed, and the cells were washed with PBS. The cells were then fixed with 4 % paraformaldehyde for 30 min, followed by neutralization with 2 mg/ml glycine for 5 min. Thereafter, the cells were permeabilized using 0.5 % Triton X, and treated with 1 × Apollo solution and DAPI for 30 min in the dark at room temperature. Images were captured using an Olympus LX71 fluorescence inverted microscope (Olympus, Tokyo, Japan).

2.9. Cell apoptosis determination

KGN cells were seeded in 6-well plates at a density of 5 × 105 cells/well. Following treatment, the cells were collected and resuspended in binding buffer. Annexin V-FITC and PI (Servicebio, Wuhan, China), were added to the cell suspension and incubated in the dark for 15 min. Subsequently, cell apoptosis was analysed using Flow cytometry (BD FACSCalibur, NJ, USA).

Additionally, cell apoptosis was measured through terminal deoxynucleotidyl transferase-dT-mediated dUTP nick end labelling (TUNEL) analysis. In brief, KGN cells were washed with PBS and then fixed with 4 % paraformaldehyde for 20 min. This was followed by permeabilization. If ovarian slices were to be examined, they were incubated with 20 μg/ml of proteinase K at room temperature for 15 min. Following a 60-min incubation with the TUNEL assay mixture (Servicebio, Wuhan, China), DAPI restaining was performed. TUNEL stained cells were then observed and photographed using the Imager D2 fluorescence microscope (Carl Zeiss Microscopy GmbH, Jena, Germany).

2.10. Western blot analysis

Cells were lysed in the ice-cold Radioimmunoprecipitation Assay (RIPA) buffer, composed of 1 × phenylmethanesulfonyl fluoride (PMSF), 1 × protease inhibitor cocktail, and 1 × phosphatase inhibitor (Beyotime, Shanghai, China). Lysates were cleared by centrifugation for 15 min at 13,000 rpm and 4 °C, and the protein concentration in the supernatant was evaluated using the Bicinchoninic Acid (BCA) protein assay kit (Beyotime). The proteins in the lysate were then separated by Sodium Dodecyl Sulfate-Polyacrylamide Gel Electrophoresis (SDS-PAGE) on 8%–12 % polyacrylamide gels and transferred onto a Polyvinylidene Fluoride (PVDF) membrane (Bio-Rad Laboratories, Hercules, CA, USA). The membrane was blocked with 5 % Bovine Serum Albumin (BSA) for an hour at room temperature before it was incubated overnight with the primary antibodies at 4 °C. It was then washed three times for 10 min each with a Tris-buffered saline containing 0.1 % Tween 20 (TBST), followed by a 1-h incubation at room temperature with the horseradish peroxidase (HRP-) conjugated secondary antibodies (Cell Signaling Technology (CST, Beverly, MA, USA). The membrane was subsequently washed three times with TBST and immunoreactive proteins were visualized using the Clarity Western Enhanced Chemiluminescence (ECL) substrate (Bio-Rad Laboratories). Band intensity was analysed and normalized using the ImageJ software. The following primary antibodies were used: PTEN (22034-1-AP, Proteintech), Akt (60203-2-Ig, Proteintech), phospho-Akt (Ser473) (66444-1-Ig, Proteintech), caspase-3 (9662, CST), cleaved caspase-3 (Asp175) (9664, CST), Bax (50599-2-Ig, Proteintech), Bcl-2 (15071, CST), CD63 (25682-1-AP, Proteintech), TSG101 (72312, CST), calnexin (10427-2-AP, Proteintech). The ladder used was MP201-01, Vazyme.

2.11. Collection of MSC-Exo

Human umbilical cord mesenchymal stem cells (hUMSCs) were acquired from the Nanfang Hospital of Southern Medical University, having secured informed consent from the donors prior to procuring full-term umbilical cords. The acquired umbilical cords were cleaned with PBS, mechanically crushed, and then cultured in DMEM/F-12 supplemented with 10 % fetal bovine serum, in a 37 °C humidified incubator with 5 % CO_2. To verify the phenotype of the hUMSCs, cell morphology was observed under optical microscope. Alizarin Red staining and Oil Red O staining were utilized to assess the differentiation ability into adipocytes and osteocytes. Flow cytometry was used to detect the cell surface hUMSCs markers CD45, CD73, and CD90. hUMSCs were cultured to the 3rd to 5th generation, the exosome-free serum and culture medium were replaced, and continue to culture for 48 h. The culture medium was collected and MSC-Exo were isolated by ultracentrifugation as previously described. MSC-Exo was identified by Western blotting, TEM and nanoFCM.

2.12. Preparation of Agomir21-Exo by electroporation

Agomir21-Exo is defined as MSC-Exo loaded with miR-21 agomir. The CUY21EDIT II electroporation system (BEX, Japan) was utilized to efficiently load Agomir-21 into MSC-Exo. Briefly, 1 μmol of Agomir-21 and 100 μl of MSC-Exo suspension were mixed into electroporation buffer solution (consisting of 1.15 mM potassium phosphate (pH 7.2), 25 mM potassium chloride, and a 21 % OptiPrep working solution). The mixture was then added to a prechilled electroporation cup. The electroporation process was carried out for 10 cycles under conditions of the perforation voltage set at 110 V, a perforation opening time of 6 ms, a perforation interval of 10 ms, a penetration voltage of 25 V, and a capacitance of 940 μF. After electroporation, the electroporation cup was immediately cooled, and the mixture was then transferred to an

Eppendorf tube and incubated at 37 °C for 1 h to restore the stability of the exosome membrane. Finally, the unloaded Agomir-21 was removed by ultracentrifugation, and Agomir21-Exo was obtained.

2.13. Preparation of GelMA hydrogel and DMPC liposomes

First, 20 ml of PBS was added to a light-protected bottle containing the initiator LAP (EFL, Suzhou, China). The mixture was then placed in a light-protected water bath at 50 °C for 15 min. During this time, the bottle was shaken every few minutes until the powder was completely dissolved, thus obtaining a 0.25 % (w/v) initiator standard solution. Subsequently, 150 mg of GelMA (EFL-GM-60, Suzhou, China) and 1 ml of the initiator standard solution were combined in a light-protected tube. The mixture was then put in a water bath at 60 °C for 30 min, during which it was agitated every 10 min to ensure homogeneity. This resulted in a 15 % (w/v) GelMA solution. Following similar steps, GelMA solutions ranging from 5 to 20 % could be produced. For safety and sterility, the GelMA solution was immediately filtered through a sterile 0.22 μm syringe filter. Furthermore, DMPC (Sigma-Aldrich, MO, USA) was dissolved in PBS at 30 °C and was sonicated for 15 min to prepare dispersed liposomes with a final concentration of 45 mM.

2.14. Preparing GelMA-Ag21Exo microspheres based on microfluidic devices

The microfluidic chips were procured from FluidicLab (Shanghai, China). Concisely, the chip was structured with three pinheads attached to the pipe separately, constituting the oil phase input, the water phase input, and the output pathway (Fig. 4A). The GelMA solution, together with the sequentially added DPMC dispersed liposomes and Agomir21-Exo was combined to form the water phase. The oil phase was constructed by uniformly mixing Mineral oil: Span 80 (Aladdin, Shanghai, China) at a ratio of 19:1 (v/v). The output path was continually irradiated with ultraviolet (UV) light.

Before initiation, the pipeline was rinsed with PBS. The oil and water phases were drawn up using 10 ml and 1 ml syringes respectively, and the liquid flow rate of the syringes was adjusted using a syringe pump (CIF, Beijing, China). Once the pump was activated, the oil and water phases were concurrently injected into the microfluidic chip at flow rates of 200 μl/min and 30 μl/min respectively. The oil phase rapidly flowed within the microfluidic chip through a designated pathway. Shear stress generated at its confluence with the water phase fractures the latter into droplets. These droplets were subsequently conveyed to the output pathway where they were photo-cross-linked and solidified into hydrogel microspheres under UV exposure. The resulting mixed hydrogel microspheres were called GelMA-Ag21Exo. Finally, the morphology of GelMA-Ag21Exo was examined with the BX63 fluorescence microscope (Olympus, Tokyo, Japan), and three-dimensional reconstruction was performed using a Zeiss LSM 880 with the Airyscan confocal microscope (Carl Zeiss Microscopy GmbH, Jena, Germany). After freeze-drying, GelMA-Ag21Exo was evaluated using the Sigma300 scanning electron microscope (SEM) (Carl Zeiss Microscopy GmbH, Jena, Germany).

2.15. Encapsulation and drug-loading efficiency of GelMA hydrogel microspheres

A specific weight of Agomir21-Exo (Wa) was utilized for the construction of GelMA hydrogel microspheres. After cleaning with PBS, the microspheres were dehydrated and dried, and the total weight (Wb) was measured. These microspheres were then thoroughly destroyed using a grinding device and centrifuged to obtain the supernatant. RIPA buffer was added to the supernatant to dissolve the exosome membrane. The concentration of exosome protein was determined using the BCA method, which helped quantify the actual weight of Agomir21-Exo encapsulated in the microspheres (Wc). The encapsulation efficiency was calculated as follows: encapsulation efficiency (%) = $W_a/W_c \times 100$. The drug loading efficiency was determined as follows: Drug loading efficiency (%) = $W_a/W_b \times 100$.

2.16. Degradation and release of GelMA hydrogel microspheres

The following experimental procedure involved the immersion of GelMA hydrogel microspheres at concentrations of 5 %, 10 %, 15 %, and 20 % (w/v), with each group weighing 10 mg. The samples were then cultured at 37 °C in a humidified incubator with 5 % CO_2. The supernatant was extracted daily to harvest exosome protein, the concentration of which was evaluated using the BCA method to construct the release curve of Agomir21-Exo. The number of remaining microspheres was recorded every 48 h, and their morphology was assessed with an Imager D2 fluorescence microscope. Afterward, the microspheres were dehydrated and dried before their weight was recorded, enabling the analysis of the rate at which the microspheres degraded.

2.17. Examining the injectability of GelMA hydrogel microspheres

A 1 ml syringe was used to aspirate approximately 0.5 ml of the microspheres, and a 24G needle was used. The evacuation of any air inside the syringe and excess PBS was ensured. After the syringe was firmly secured on the workstation, the thrust probe of a push-pull force meter (Sanliang, Shanghai, China) was used to consistently and steadily compel the syringe until microspheres were extruded from the needle tip. At this time, the value on the push-pull force meter was recorded for each 1 mm length progressed and this measurement process was replicated 20 times.

2.18. Uptake of Agomir21-Exo by KGN cells

First, the dosage of Agomir21-Exo was adjusted according to the previously calculated encapsulation efficiency of hydrogel to balance the effective exosome concentrations of GelMA-Ag21Exo and Agomir21-Exo. The GelMA-Ag21Exo microspheres containing 10 μg of Agomir21-Exo were placed in a Transwell chamber and incubated with KGN cells at 37 °C. Cells treated with 10 μg Agomir21-Exo served as the control. The cells were observed every 48 h using a fluorescence microscope.

2.19. Animal treatments

All experiments were conducted using ten-week-old C57BL/6 mice. The animals were purchased from the Laboratory Animal Center of Southern Medical University (Guangzhou, China). All experimental procedures received ethical approval from the Laboratory Animal Center of Southern Medical University. All mice were provided with a standard diet and water and housed under a 12/12-h light/dark cycle.

Female mice were injected with 4-vinylcyclohexene diepoxide (VCD) (80 mg/kg) for 10 consecutive days to induce POI. An important mechanism of VCD-induced POI is the induction of GC apoptosis, which leads to the destruction of primordial and primary follicles [28,29]. The control mice were injected with the same amount of saline solution for 10 consecutive days. To salvage the VCD-induced ovarian damage, the MSC-Exo group and the Agomir21-Exo group were administered 200 μg of MSC-Exo and Agomir21-Exo respectively, via intraperitoneal injection into POI mice. Based on an analysis of drug-loading efficiency, the mass of microspheres loaded with 200 μg of Agomir21-Exo was approximately 5 mg. Thus, in the GelMA-Ag21Exo group, 5 mg of GelMA-Ag21Exo microspheres was intraperitoneally injected. All these treatments were repeated every 7 days over a therapeutic period of 21 days.

2.20. In vivo fluorescence imaging

The fluorescent labelling of Agomir21-Exo was accomplished by

using Dil. Each mouse in the Agomir21-Exo group was administered 100 μg of Agomir21-Exo, while those in the GelMA-Ag21Exo group were given 2.5 mg of GelMA-Ag21Exo microspheres. The assessment of fluorescence was conducted on days 1, 3, 5, and 7 with the Spectral AMI *in vivo* imaging system (Spectral Instruments Imaging, AZ, USA). This procedure was performed both *in vivo* and with respect to the female reproductive system. Finally, the ovaries were harvested and homogenized for RNA extraction. The levels of miR-21 were subsequently evaluated using qRT-PCR.

2.21. Ovarian morphological analysis and follicle counting

Ovaries were fixed in 4 % paraformaldehyde for 24 h, dehydrated in ethanol, and embedded in paraffin wax. Sections 4 μm thick were deparaffinized with xylene and stained with Hematoxylin and Eosin (H&E) following standard protocols for follicle assessment. A follicle containing an oocyte with a distinct nucleus was counted and classified as a primordial, primary, secondary and antral according to previously described criteria [30]. The number of follicles was calculated from the total counts of three representative ovarian midsections of each rat.

2.22. Immunohistochemical analysis

Ovarian tissue sections of 4 μm thickness were dewaxed in xylene and rehydrated in a graded series of alcohols. Following antigen retrieval, endogenous peroxidase activity was blocked with 3 % hydrogen peroxide. The sections were then incubated in serum for blocking, followed by overnight incubation with primary antibodies PTEN (22034-1-AP, Proteintech), phospho-Akt (Ser473) (66444-1-Ig, Proteintech), cleaved caspase-3 (Asp175) (9664, CST), and Bax (50599-2-Ig, Proteintech) at 4 °C. Subsequently, the sections were incubated with secondary antibody and treated with a diaminobenzidine (DAB) staining kit (Zhongshanjinqiao, Beijing, China). The slides were examined under an Olympus BX63 microscope.

2.23. Detection of the estrous cycle

The estrous cycle was evaluated through vaginal smears for a continuous period of 30 days. After the mouse's vaginal orifice was cleaned with physiological saline solution, the exfoliated epithelial cells were collected and applied to a glass slide. The smear was allowed to air dry, after which, it was stained with methylene blue. The cell types and their proportions were then quantified under a microscope.

2.24. Serum hormone measurement with Enzyme-linked immunosorbent assay (ELISA)

Mouse blood samples were preserved overnight at 4 °C, followed by centrifugation at 3000×*g* for 10 min and the serum was subsequently frozen at −80 °C until assessment. The mouse serum levels of AMH (ml037597, Enzyme-linked Biotechnology, Shanghai, China), FSH (ml001910, Enzyme-linked Biotechnology), estradiol (E2) (ml001962, Enzyme-linked Biotechnology), C-Reactive Protein (CRP) (KE10128, Proteintech), TNF-α (KE10002, Proteintech) and IL-1 (KE10003, Proteintech) were measured with ELISA kits. The mouse serum levels of Alanine aminotransferase (ALT), Aspartate Aminotransferase (AST) and Serum creatinine (SCr) were measured with Fully automated biochemical analyzer (AU800, Olympus, Tokyo, Japan).

2.25. Fertility test

Female mice were mated with fertile male C57BL/6 mice at a ratio of 1:2 for 3 months after treatment. Pregnancy and parturition were monitored and recorded weekly for each female mouse. Additionally, male mice were rotated randomly among cages each month.

2.26. Statistical analysis

Statistical analysis was conducted using SPSS 22.0 software, with numerical data expressed as mean ± standard deviation (SD). Student's t-test was applied to assess statistical differences between two groups. The non-parametric Kruskal-Wallis test was used where appropriate. A p-value less than 0.05 was considered to indicate statistical significance.

3. Results

3.1. The miR-21 carried by FF-Exo may be associated with GC apoptosis in patients with POI

To identify potentially therapeutic exosomal miRNAs, we collected and isolated FF-Exo from both patients with normal ovarian reserve and those suffering from POI. We then examined the morphology and phenotype of FF-Exo based on exosome characteristics. TEM revealed that the FF-Exo from both the normal and POI groups were cup-shaped vesicles with a bilayer membrane structure (Fig. 1A). The size distributions of the within Nomal-FF-Exo and POI-FF-Exo, as observed through nanoFCM, were relatively similar, at 77.0 ± 19.6 nm and 80.4 ± 21.7 nm respectively (Fig. 1B). However, the average particle concentration in the POI-FF-Exo was significantly lower than that in the Nomal-FF-Exo (Fig. 1C). This suggested that intrafollicular communication might be compromised. Both positive exosomal markers (CD63 and TSG101) and negative exosomal marker (calnexin) were expressed in the FF-Exo the from two groups (Fig. 1D).

To further investigate the impact of POI-FF-Exo on hGCs, we added 20 μg of FF-Exo into 1×10^5 hGCs. The Dil-tagged exosomes exhibited red fluorescence in the cytoplasm (Fig. 1E), indicating the uptake of FF-Exo by hGCs. After co-incubation for 96 h, CCK-8 revealed significant growth inhibition in hGCs of the POI-FF-Exo group (Fig. 1F); Flow cytometry demonstrated a notably greater percentage of apoptotic hGCs in the POI-FF-Exo group than in the Normal-FF-Exo group (8.74 ± 1.57 % and 4.04 ± 0.79 %, respectively) (Fig. 1G and H). These results suggest functional differences between POI-FF-Exo and Normal-FF-Exo. Furthermore, within the context of similar morphologies and particle sizes, such functional differences potentially indicate variations in the cargo carried by POI-FF-Exo and Normal-FF-Exo.

Exosomes, as signalling intermediaries rich in miRNA molecules, present intriguing research potential [31]. To further explore the mechanism by which POI-FF-Exo induce apoptosis in hCGs, we extracted total RNA from three pairs of Normal-FF-Exo and POI-FF-Exo and studied their miRNA profiles via high-throughput miRNA sequencing. The results revealed a significant increase in 70 miRNAs and a significant decrease in 150 miRNAs in POI-FF-Exo ($|\log2(\text{Fold Change})| > 2$ and P-value<0.05) (Fig. 1I). The top 50 differentially expressed miRNAs are shown in a heatmap (Fig. 1J). A high expression abundance of miRNAs usually indicates widespread and profound regulation. According to our sequencing results, miR-21 (miR-21-5p) demonstrated the highest expression abundance among the differentially expressed miRNAs (Fig. 1K), which has been widely reported to be associated with cell apoptosis and POI [32–34]. Owing to the difficulty of collecting follicular fluid from POI patients, we collected FF-Exo from bPOI patients which is at early-stage of POI for validation. Further qRT-PCR revealed a significant reduction in miR-21 in the FF-Exo of bPOI patients (Fig. 1L), which was consistent with the sequencing results. These results show that miR-21 is highly enriched in FF-Exo, making it one of the major cargoes carried by FF-Exo, and it has significant altered in POI. This finding suggested that miR-21, a natural miRNA loaded in exosomes, could be associated with GC apoptosis in patients with POI.

3.2. miR-21 regulates the proliferation and apoptosis of GCs through the PTEN/akt pathway

The PTEN/Akt pathway is crucial for follicle development [35].

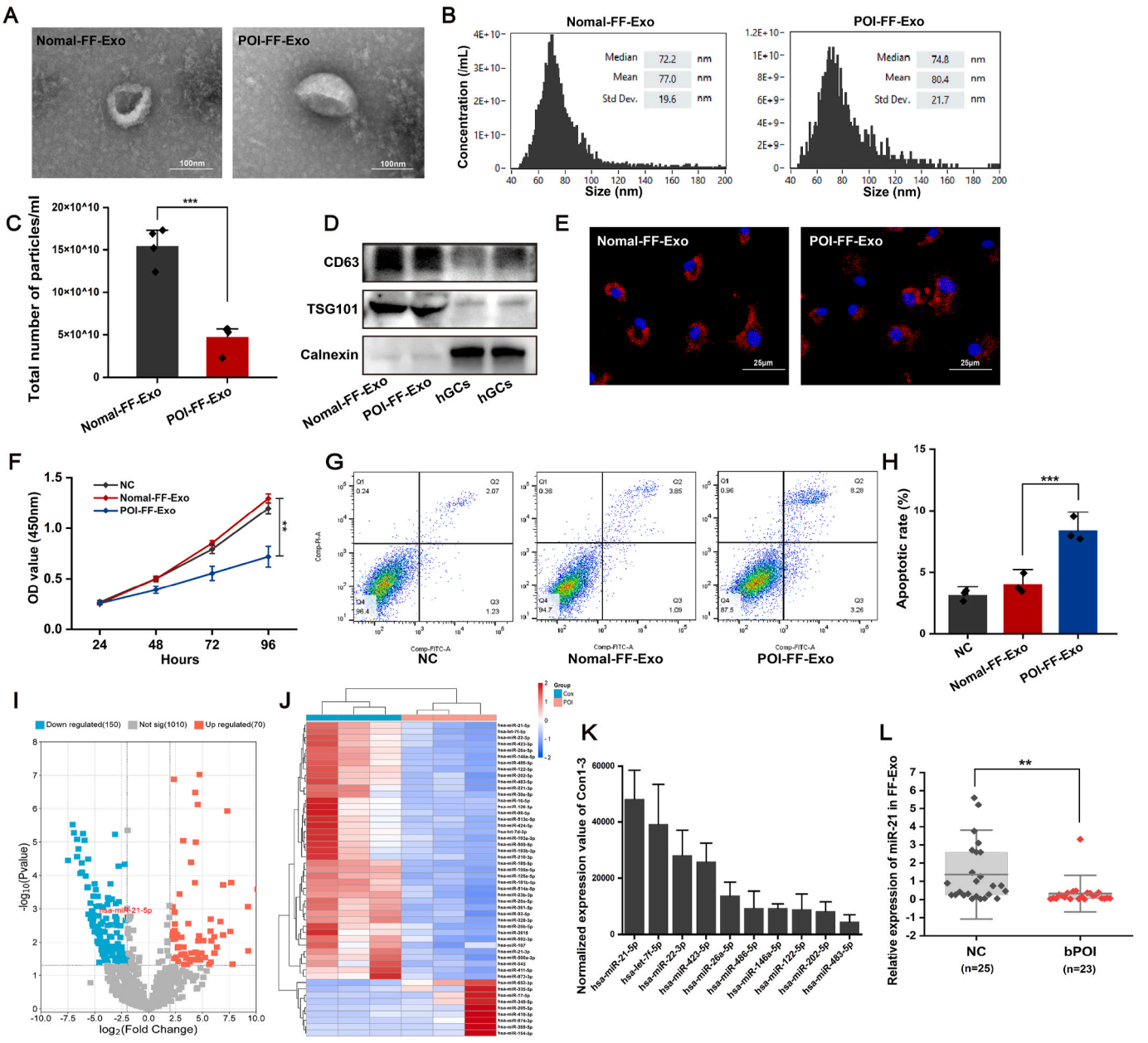

Fig. 1. miR-21 was identified as the predominant miRNA with low-expression in POI-FF-Exo. (A) TEM images of Normal-FF-Exo and POI-FF-Exo. (B) Exosome particle size distributions of Normal-FF-Exo and POI-FF-Exo, measured with nanoFCM. (C) Differences in the concentrations of Normal-FF-Exo and POI-FF-Exo detected by nanoFCM. (D) Expression of exosomal markers (CD63, TSG101 and calnexin) analysed by Western blot. (E) Dil-tagged FF-Exo (RED) were taken up by hGCs (BLUE). (F) CCK-8 assay was used to examine the proliferation of hGCs treated with Normal-FF-Exo and POI-FF-Exo within 24–96 h, and the absorbance at 450 nm was measured. (G, H) Apoptosis levels at 72 h after different treatments in hCGs were analysed using Flow cytometry; the percentages of apoptotic cells in the NC group, Normal-FF-Exo group, and POI-FF-Exo group were 3.14 ± 0.45 %, 4.04 ± 0.79 %, and 8.74 ± 1.57 %, respectively. (I) Volcano plot of the expression levels of all known miRNAs determined by high-throughput sequencing. (J) Heatmap showing the 50 most abundantly expressed miRNAs among differentially expressed miRNAs. (K) The top 10 abundantly expressed miRNAs presented within a Normalized Value framework from miRDeep2 software. (L) Differences in the expression levels of miR-21 in FF-Exo samples from 25 control patients and 23 bPOI patients, were analysed by qRT-PCR.
Notes: The data are presented as mean ± standard deviation (SD) from at least three independent experiments. *P < 0.05, **P < 0.01, ***P < 0.001.
Abbreviations: Normal-FF-Exo, follicular fluid exosomes in patients with normal ovarian reserve; POI-FF-Exo, follicular fluid exosomes in patients with POI.

PTEN was predicted to be a target gene of miR-21 (Fig. 2A), and its regulatory role was validated by dual luciferase assay in 293T cells (Fig. 2B). To explore the mechanism underlying the effect of miR-21 on GCs, we selected the KGN cell line for *in vitro* experiments. Under the influence of the miR-21 antagonist Antagomir-21, the protein expression of PTEN was significantly upregulated, and under the influence of the miR-21 agonist Agomir-21, the protein expression of PTEN was notably downregulated (Fig. 2C). We further constructed siPTEN, which effectively knocked down the expression of the PTEN gene (Fig. 2D). Western blot analysis demonstrated that PTEN protein expression was increased in KGN cells treated with Antagomir-21, while the p-Akt protein expression was significantly decreased; however, this suppression could be effectively reversed by the action of siPTEN (Fig. 2E–G). These results suggested that the positive regulation of Akt by miR-21 was dependent on the inhibition of PTEN. Subsequently, we tested the expression of the apoptosis-related protein Bcl-2, Bax and cleaved caspase-3. Following treatment with Antagomir-21, the expression of Bax and cleaved caspase-3 in KGN cells was elevated, while Bcl-2 expression was

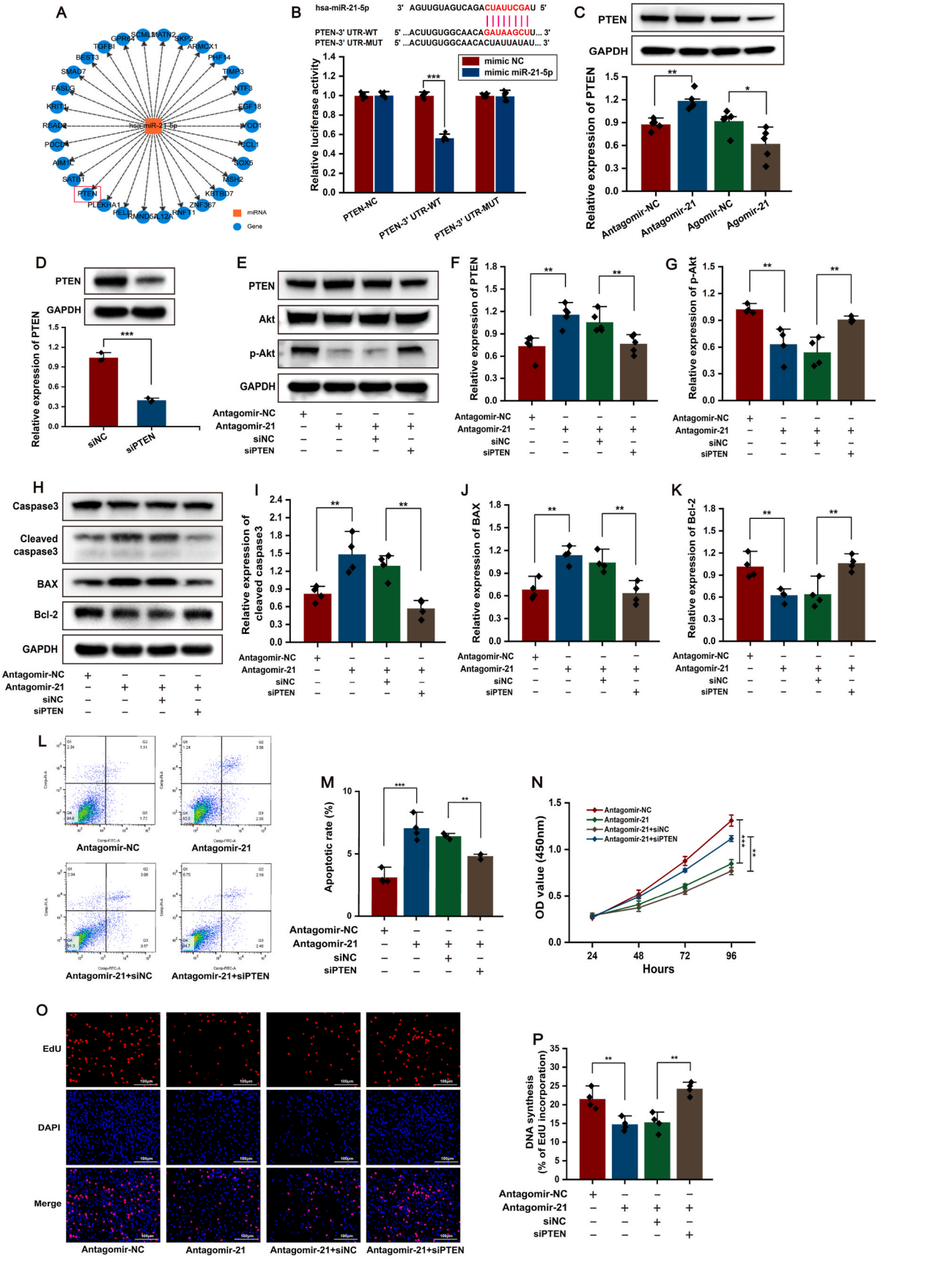

(caption on next page)

Fig. 2. miR-21 regulates the proliferation and apoptosis of KGN cells. (A) The prediction of miR-21's target genes by TargetScan. (B) The presence of potential miR-21 binding sites in the 3′-UTR of PTEN mRNA, as determined by dual luciferase assay, confirmed the interaction between miR-21 and PTEN. (C) The effects of Antagomir-21 and Agomir-21 on the expression of the PTEN protein were assessed using Western blotting. (D) The efficiency of siPTEN knocking down the expression of the PTEN protein in KGN cells. (E–G) The effects of four different treatments, Antagomir-NC, Antagomir-21, Antagomir-21+siNC, and Antagomir-21+siPTEN, on the protein expression of PTEN, Akt, p-Akt, GAPDH were evaluated by Western blotting. (H–K) Western blotting was also used to determine the effects of the aforementioned four treatments on the protein expression of Bax, Bcl-2, caspase-3, cleaved caspase-3 and GAPDH. (L, M) The induction of apoptosis in KGN cells by the aforementioned four treatments was evaluated using Flow cytometry, with the apoptosis rates calculated as 3.12 ± 0.55 %, 7.07 ± 0.94 %, 6.43 ± 0.23 %, and 4.84 ± 0.23 %, respectively. (N) CCK-8 assay was used to examine the proliferation of KGN cells treated as described above within 24–96 h, and the absorbance at 450 nm was measured. (O, P) EdU assay was performed to determine the proliferation of KGN cells subjected to the aforementioned four treatments 48 h later; proliferating cells were detected with EdU (RED), and cell nuclei were stained with DAPI (BLUE).
Notes: The data are presented as mean ± standard deviation (SD) from at least three independent experiments. *P < 0.05, **P < 0.01, ***P < 0.001.

reduced, indicating the occurrence of apoptosis. However, apoptosis significantly decreased after PTEN knockdown (Fig. 2H–K). Flow cytometric analysis further confirmed that the regulation of KGN cell apoptosis by miR-21 was dependent on the PTEN/Akt pathway (Fig. 2L and M). The CCK-8 (Fig. 2N) and EdU (Fig. 2O and P) experiments demonstrated that the downregulation of miR-21 inhibited KGN cell proliferation, and this effect could be partly reversed by concurrently reducing PTEN expression.

To investigate the effect of Agomir-21 on GC apoptosis, we generated an apoptosis model by treating KGN cells with 1 mM VCD for 24 h (Figure S1 K). The experimental results showed that compared to Agomir-NC, Agomir-21 significantly inhibited VCD-induced apoptosis in KGN cells (Figure S1 A-F). Further rescue experiments demonstrated that Agomir-21 effectively counteracted the decrease in cell viability and apoptosis caused by PTEN protein overexpression (Figure S1 G-J).

These results indicated that lower miR-21 expression could lead to KGN cell apoptosis and proliferation inhibition, supplementation with miR-21 can reverse these effects, which was at least partially depended on the PTEN/Akt pathway. It could be predicted that supplementation with miR-21 is a way to alleviate apoptosis of GCs in POI patients.

3.3. Agomir-21 loaded in MSC-Exo can effectively inhibit VCD-induced KGN cell apoptosis

The choice of an appropriate carrier is crucial for enhancing the delivery stability of Agomir-21. Compared with FF-Exo, MSC-Exo is a natural nanocarrier that is widely derived, easy to culture and extract, has multiple inherent therapeutic functions, including immunoregulation, anti-inflammatory effects, and tissue regeneration [36]. Therefore, as a promising miRNA carrier, MSC-Exo has emerged as a novel therapy for numerous diseases [8,15]. In this study, we selected and cultured hUMSCs to extract MSC-Exo. By the third-generation, the typical fusiform adherent growth morphology could be clearly observed under an optical microscope (Figure S2 A). Oil Red O staining was utilized following the induction of adipogenesis in hUMSCs, and orange-red lipid droplets were observed under the optical microscope, indicating the adipogenic potential of the cultured hUMSCs (Figure S2 A). Upon osteogenic induction, alizarin red solution was applied for calcium deposition staining, and the observation of deep red calcium nodules verified the osteogenic capability of the cultured hUMSCs (Figure S2 A). Relevantly, the chondrogenic potential of hUMSCs was demonstrated through Alcian blue staining (Figure S2 A). Then, we used Flow cytometry to detect MSC surface markers. As expected, CD34 (0.17 %) and CD45 (0.05 %) was negative, while CD73 (99.5 %), CD90 (95.1 %) and CD105 (99.9 %) were positive (Figure S2 B). MSC-Exo was extracted from the supernatant of 3rd-to 5th-generation cultured hUMSCs using ultracentrifugation. Similar to FF-Exo, MSC-Exo was identified via TEM (Figure S2 C), nanoFCM (Figure S2 D) and Western blotting (Figure S2 E). The results obtained were consistent with the characteristics of MSC-Exo.

Electroporation, a process that relies on exposing the exosome membrane to high-intensity electrical pulses, is a highly efficient method for loading materials such as miRNA [37,38]. In this study, we utilized an electroporator to effectively load FAM-labelled Agomir-21 into Dil-labelled MSC-Exo at a perforation voltage of 110 V. As a control, an equivalent quantity of FAM-agomir21 was co-cultivated in the MSC-Exo solution for 4 h at 37 °C, after which the unloaded FAM-agomir21 was removed from both groups using ultracentrifugation, resulting in Agomir21-Exo. For the convenience of observation, we added Agomir21-Exo to KGN cells. Fluorescence microscopy revealed a significantly greater intensity of green fluorescence from Agomir-21 in the electroporation group than in the cocultivation group, while the red fluorescence intensities from the MSC-Exo were similar in both groups (Fig. 3A). This finding suggested that Agomir-21 was more efficiently loaded into MSC-Exo through electroporation. Next, we extracted total RNA from the Agomir21-Exo of both groups for qRT-PCR analysis of miR-21 expression level (Fig. 3B). The results confirmed the increased transfection efficiency of the electroporation method.

To investigate the effect of Agomir21-Exo on GC apoptosis, we generated an apoptosis model by treating KGN cells with 1 mM VCD for 24 h. We subsequently added 20 μg of MSC-Exo or Agomir21-Exo to approximately 1×10^5 apoptotic KGN cells, cultured them for 48 h, and then collected the cells for detection. Western blot results demonstrated that both MSC-Exo and Agomir21-Exo inhibited the overexpression of PTEN induced by VCD, thereby activating p-Akt (Fig. 3C–E) and ultimately suppressing KGN cell apoptosis (as indicated by decreased expression levels of Bax and cleaved caspase-3 and increased expression level of Bcl-2) (Fig. 3F–I). Specifically, the inhibitory effect of Agomir21-Exo on the PTEN/akt pathway and apoptosis was significantly greater than that of MSC-Exo (Fig. 3C–I), which was attributed to the loaded Agomir-21. However, this inhibitory effect of Agomir21-Exo could be markedly reversed by LY294002 (Fig. 3C–I), a PI3K inhibitor that can inhibit Akt activation. These results suggest that Agomir21-Exo delivers Agomir-21 to inhibit the PTEN/Akt pathway and ultimately suppresses apoptosis in KGN cells. Flow cytometry analysis showed that Agomir21-Exo could reduce VCD-induced apoptosis of KGN cells, and the therapeutic effect was stronger than that of MSC-Exo (Fig. 3J and K). We further validated the therapeutic effect of Agomir21-Exo through TUNEL staining. The results showed that the number of TUNEL-positive cells (GREEN) in the VCD + Agomir21-Exo group was significantly lower than that in the VCD + MSC-Exo and VCD groups (Fig. 3L and M), indicating that Agomir21-Exo could effectively rescue KGN cells from VCD-induced apoptosis and serve as a small molecule drug for exosome-based therapeutics.

3.4. Construction of DPMC-GelMA hydrogel microspheres for encapsulating Agomir21-Exo

To enhance the stability and long-term retention of Agomir21-Exo *in vivo*, we prepared GelMA hydrogel microspheres by photopolymerization of GelMA hydrogel doped with Agomir21-Exo based on microfluidic technology. Concurrently, drawing on the report from Lin W et al. [25], we incorporated DMPC liposomes into GelMA with the aim to reduce friction between hydrogel microspheres and improve injectability. The schematic diagram of the process is shown in Fig. 4A.

Fig. 4B shows the morphological difference between lipid-free GelMA microspheres (Lipid-free GelMA) and those incorporated with DMPC (DMPC-GelMA), where visible aggregation was observed in

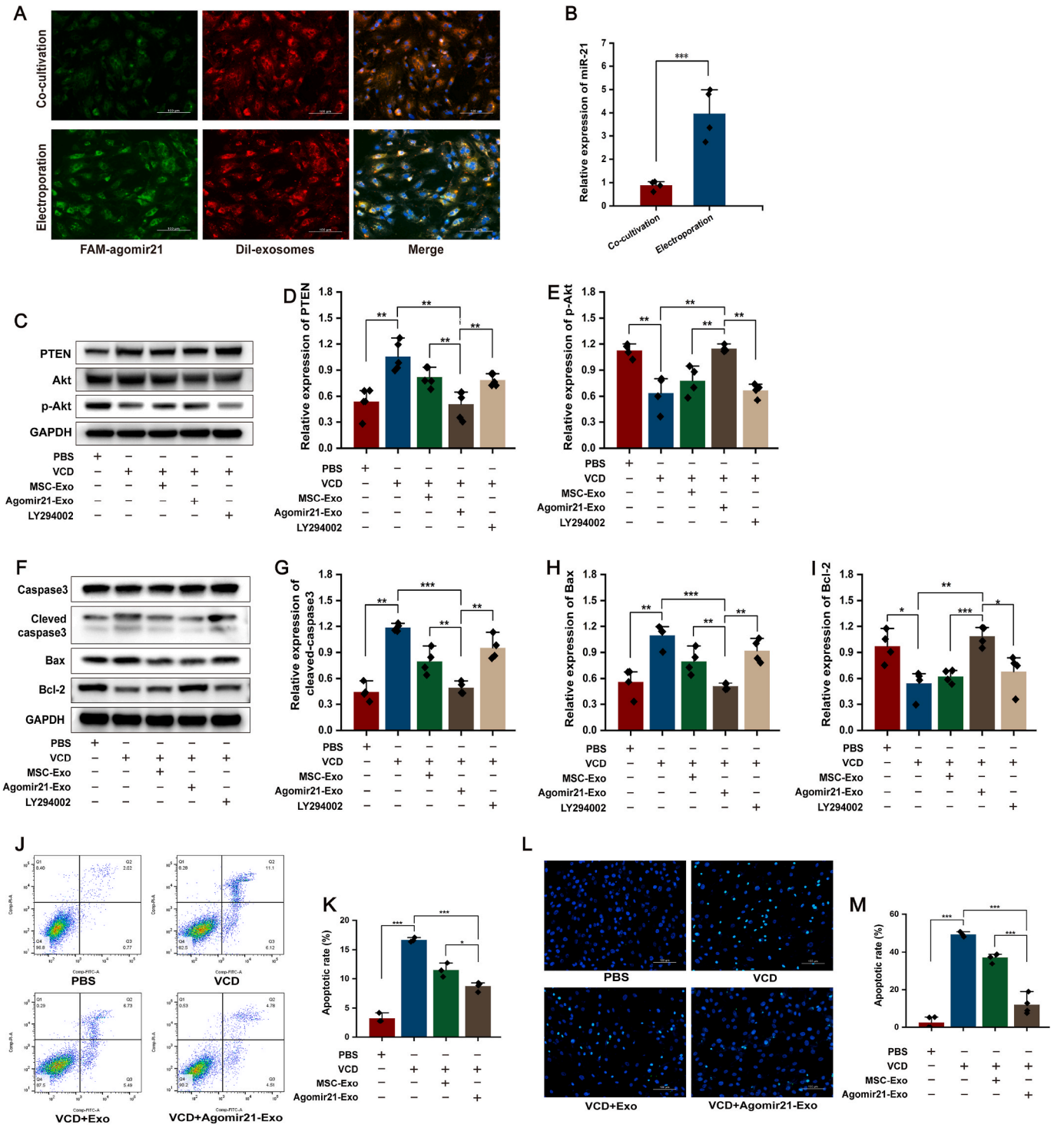

Fig. 3. Inhibitory effect of Agomir21-Exo on apoptosis of KGN cells. (A) Representative micrographs showing differences in the transfection efficiency of co-cultivation and electroporation of Agomir-21. Transfected Agomir-21 was labelled with FAM (GREEN), MSC-Exo was labelled with Dil (RED), and cell nuclei were labelled with DAPI (BLUE). (B) qRT-PCR analyses showing the expression level of normalized Agomir-21 in the co-cultivation and electroporation groups. (C–E) Western blot analyses showing the protein expression levels of PTEN and p-Akt in the five groups: PBS, VCD, VCD + MSC-Exo, VCD + Agomir21-Exo and VCD + Agomir21-Exo + LY294002. (F–I) Western blot analyses showing the protein expression levels of cleaved caspase-3, Bax, and Bcl-2 in the aforementioned five groups. (J, K) Flow cytometry showing the percentages of apoptotic cells in the four groups: PBS, VCD, VCD + MSC-Exo, and VCD + Agomir21-Exo, which were 3.25 ± 0.81 %, 16.67 ± 0.36 %, 11.49 ± 1.2 %, and 8.74 ± 0.71 %, respectively. (L, M) TUNEL staining showing the numbers of apoptotic cells in the aforementioned four groups. Apoptotic cell nuclei were labelled with dUTP (GREEN), and all cell nuclei were labelled with DAPI (BLUE).

Notes: The data are presented as mean ± standard deviation (SD) from at least three independent experiments. *P < 0.05, **P < 0.01, ***P < 0.001.

Abbreviations: VCD, 4-vinylcyclohexene diepoxide; MSC-Exo, mesenchymal stem cell-derived exosomes; Agomir21-Exo, MSC-Exo loaded with miR-21 agomir.

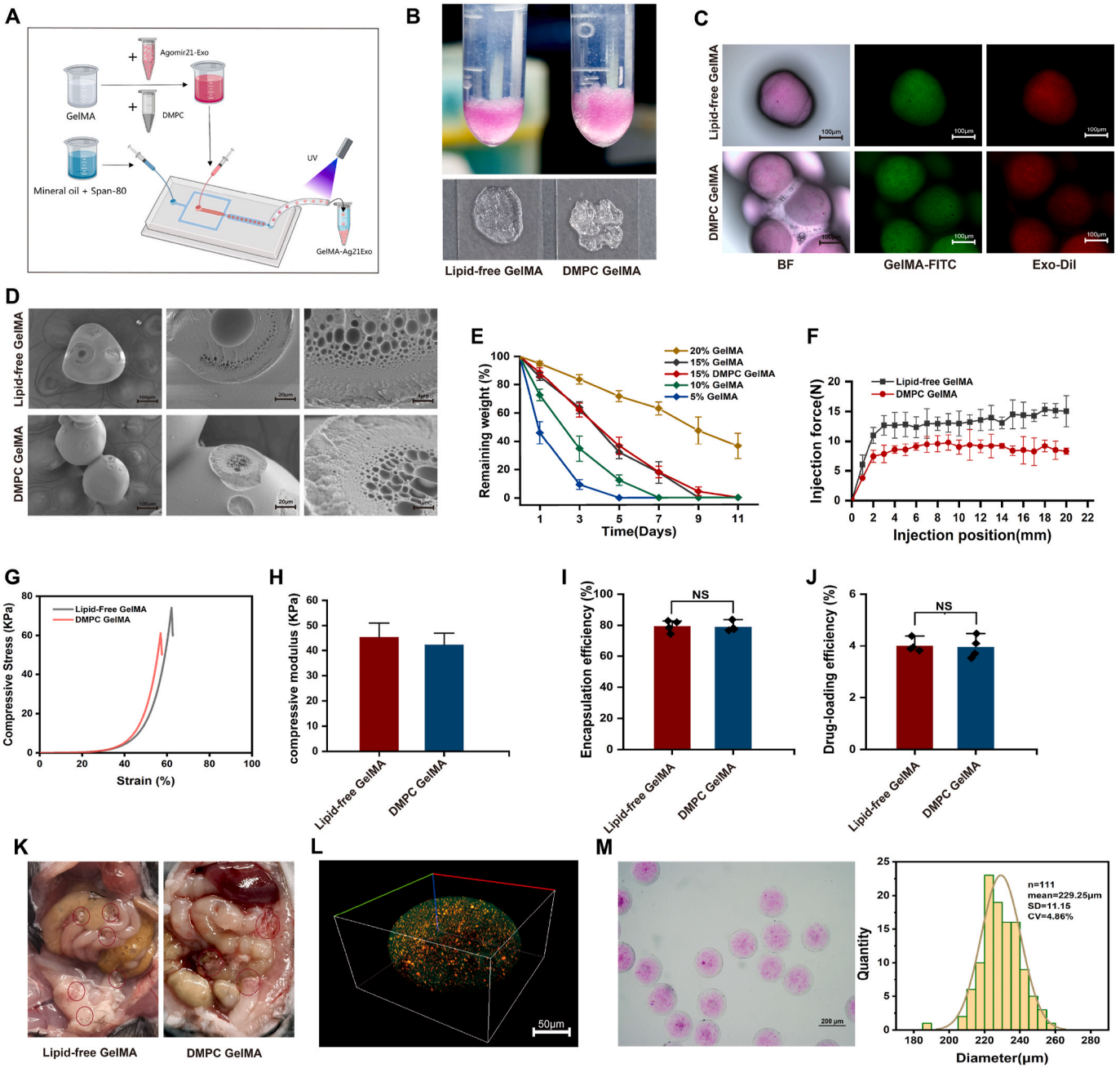

Fig. 4. Properties of GelMA-Ag21Exo. (A) Schematic diagram of the fabrication process for GelMA-Ag21Exo using microfluidic techniques. (B) The visual appearance of Lipid-free GelMA and DMPC-GelMA. (C) Microstructures of Lipid-free GelMA and DMPC-GelMA observed under a fluorescence microscope, with GelMA tagged with green fluorescence and Agomir21-Exo tagged with red fluorescence. (D) SEM images of Lipid-free GelMA and DMPC-GelMA. (E) Degradation curves of GelMA microspheres at concentrations of 5 %, 10 %, 15 % and 20 %, as well as 15 % DMPC-GelMA. (F) The necessary pushing force for microsphere extrusion from a needle as measured by a push-pull force meter. (G) Compressive stress–strain curves of Lipid-free GelMA and DMPC-GelMA. (H) Compressive modulus of Lipid-free GelMA and DMPC-GelMA. (I) encapsulation efficiency efficiency of Lipid-free GelMA and DMPC-GelMA. (J) Drug-loading efficiency of Lipid-free GelMA and DMPC-GelMA. (K) Microsphere distribution in the peritoneal cavity 3 days after the intraperitoneal injection of Lipid-free GelMA and DMPC-GelMA. (L) Three-dimensional structure of GelMA-Ag21Exo photographed using the confocal microscope. (M) The diameter distribution of GelMA-Ag21Exo was determined by optical microscopy and analysed using ImageJ software.

Notes: The data are presented as mean ± standard deviation (SD) from at least three independent experiments. *P < 0.05, **P < 0.01, ***P < 0.001.

Abbreviations: GelMA, Gelatin methacryloyl; DMPC, dimyristoylphosphatidylcholine; Lipid-free GelMA, GelMA hydrogel microspheres without any lipid; DMPC-GelMA, GelMA hydrogel microspheres with 45 mM DMPC; GelMA-Ag21Exo, the 15 % GelMA hydrogel microspheres containing 45 mM DMPC and encapsulated with Agomir21-Exo.

DMPC-GelMA. Upon further observation under a fluorescence microscope, we found that the GelMA hydrogel (GREEN) encapsulated Agomir21-Exo (RED) impeccably, and the trait of DMPC-GelMA aggregation became more obvious (Fig. 4C). The SEM image of microspheres after lyophilization are shown in Fig. 4D. Both Lipid-free GelMA and DMPC-GelMA displayed similar porous structures on their fracture surfaces, which was conducive to the attachment of small molecules such as Agomir21-Exo.

To determine the appropriate GelMA concentration, we examined decomposition rates of GelMA microspheres at 5 %, 10 %, 15 %, and 20

% concentrations (Fig. 4E). Due to their rapid decomposition and instability, GelMA at 5 % and 10 % were excluded. The 20 % GelMA was also excluded owing to its slow decomposition rate, which could potentially lead to the deactivation of encapsulated Agomir21-Exo. The 15 % GelMA, which had a decomposition period of approximately 7 days and didn't show significant changes with the addition of DMPC, was thus selected. Given the excellent injectability and roughly similar degradation and drug-loading properties of DMPC-GelMA compared to the Lipid-free GelMA, we chose 15 % DMPC-GelMA for further experiments.

Despite the seemingly enlarged volume due to aggregation, DMPC-GelMA could pass through the 24G needle more smoothly, which may be due to its flexible morphology and decreased friction, resulting in a significant reduction in the required injection force (Fig. 4F). We evaluated the Lipid-Free GelMA and DMPC GelMA through compression experiments. Fig. 4G displays typical stress-strain curves of the hydrogels. The incorporation of DMPC resulted in a slight decrease in the compressive modulus of GelMA (Fig. 4H), making it more deformable. Furthermore, we assessed the encapsulation efficiency and drug loading efficiency of both Lipid-Free GelMA and DMPC-GelMA, which were found to be 79.5 ± 3.8 % and 79.0 ± 3.1 %, as well as 4.01 ± 0.26 % and 3.95 ± 0.43 %, respectively (Fig. 4I and J).

Three days after the intraperitoneal injection of the microspheres into the mice, agglomerated DMPC-GelMA could be observed in the peritoneal cavity (Fig. 4K). We further evaluated the effects of microsphere injection on mice. There were no significant differences in liver and kidney tissue structure between mice receiving Lipid-free GelMA and DMPC-GelMA injections (Figure S3 A). Compared to the control group, both groups showed no significant differences in ALT, AST, and SCr levels (Figure S3 B-D), indicating minimal impact of microsphere injection on mouse liver and kidney function. However, serum TNF-α and IL-1β levels were elevated in the Lipid-free GelMA group compared

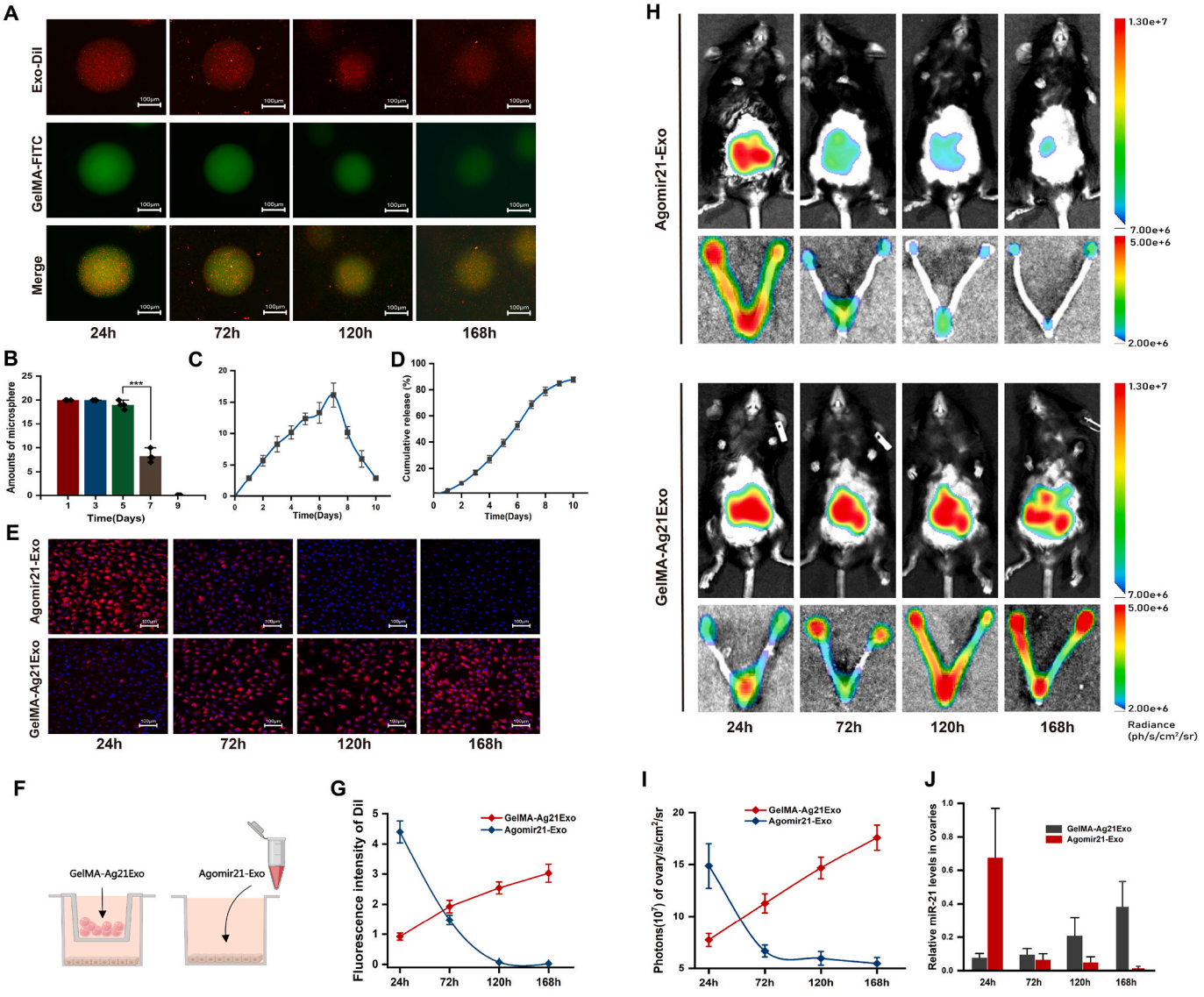

Fig. 5. Controllable sustained release capability of GelMA-Ag21Exo. (A) Decomposition images of GelMA-Ag21Exo at 37 °C over the course of 7 days. (B) Microsphere counts of GelMA-Ag21Exo at 37 °C over the course of 9 days. (C, D) The quantity and percentage of exosomes released from GelMA-Ag21Exo at 37 °C over the duration of 1–10 days. (E) Fluorescence trends of Agomir21-Exo and GelMA-Ag21Exo co-incubated with KGN cells over the course of 7 days. (F) Schematic illustration of the co-incubation. (G) Statistical graph of the trends in fluorescence changes in co-incubation. (H) Fluorescence imaging trends of Agomir21-Exo and GelMA-Ag21Exo within the whole body and reproductive organs of mice. (I) Statistical graph of the trends in fluorescence intensity changes in mouse reproductive organs. (J) Expression levels of miR-21 in mouse ovaries measured by qRT-PCR.

Notes: The data are presented as mean ± standard deviation (SD) from at least three independent experiments. *P < 0.05, **P < 0.01, ***P < 0.001.
Abbreviations: GelMA-Ag21Exo, the 15 % GelMA hydrogel microspheres containing 45 mM DMPC and encapsulated with Agomir21-Exo.

to the control group, while no significant differences were observed in the DMPC-GelMA group, suggesting that relatively aggregated DMPC-GelMA has fewer inflammatory side effects (Figure S3 E, F).

We named the 15 % GelMA hydrogel microspheres containing 45 mM DMPC and encapsulated with Agomir21-Exo as GelMA-Ag21Exo. The three-dimensional structure of GelMA-Ag21Exo was comprehensively demonstrated by confocal microscopy, with Agomir21-Exo being evenly distributed within the spherical structure (Fig. 4L). Statistical analysis revealed that the diameter distribution of GelMA-Ag21Exo was 229.25 ± 11.15 μm (Fig. 4M).

3.5. GelMA-Ag21Exo enhances the stability and long-term retention of Agomir21-Exo through sustained release

To explore the dynamic release of Agomir21-Exo from GelMA-Ag21Exo, we incubated GelMA-Ag21Exo in PBS at 37 °C. Over a period of 1–7 days, GelMA-Ag21Exo continually decomposed and gradually released the encapsulated Agomir21-Exo into the surrounding environment. By the 7th day, GelMA with green fluorescence was already difficult to clearly observe, while the viewing field was filled with the red fluorescent label of Agomir21-Exo (Fig. 5A). Counting of the microspheres demonstrated a significant reduction in their numbers by day 7, with no microspheres remaining by day 9 (Fig. 5B). During the period of 1–10 days, we collected supernatants from the decomposition of GelMA-Ag21Exo and measured the protein concentrations using the BCA method to determine the amount of released exosomes. Fig. 5C and D displays the daily exosome release curve and the cumulative percentage of release respectively. The release of exosomes increased rapidly within 1–7 days, peaked on day 7, and then promptly decreased (Fig. 5C).

To confirm that GelMA-Ag21Exo could facilitate prolonged retention of Agomir21-Exo, we added 250 μg of GelMA-Ag21Exo, which encapsulated approximately 10 μg of Agomir21-Exo, to cultured KGN cells using Transwell chambers because of the large volume of GelMA-Ag21Exo (Fig. 5F). Meanwhile, we added 10ug of Agomir21-Exo to cultured KGN cells as a control group. On the first day, the Agomir21-Exo group exhibited robust red-fluorescence. However, due to rapid depletion, the fluorescence intensity markedly decreased by the third day. In contrast, the GelMA-Ag21Exo group displayed a progressive increase in fluorescence intensity within 1–7 days and maintained this intensity over an extended period (Fig. 5E–G).

To probe the sustained release effect of GelMA-Ag21Exo *in vivo*, we intraperitoneally injected Dil-tagged Agomir21-Exo and GelMA-Ag21Exo into VCD-induced POI mice and subsequently conducted fluorescence imaging of the whole body and reproductive organs of the mice on days 1, 3, 5 and 7 (Fig. 5H). As expected, in both the Agomir21-Exo group and the GelMA-Ag21Exo group, Agomir21-Exo was successfully transferred into the damaged ovaries of POI mice. GelMA-Ag21Exo, due to its prolonged presence within the peritoneal cavity, exhibited durable and stable red fluorescence in whole-body imaging. The intensity of fluorescence in reproductive organs tended to be similar to that in cell lines; the fluorescence intensity in the Agomir21-Exo group rapidly decreased following an initial peak on the first day, while the fluorescence intensity in the GelMA-Ag21Exo group gradually increased, maintaining a relatively high level (Fig. 5I). Finally, we collected ovaries from the mice used for fluorescence imaging and extracted ovarian RNA to assess the expression levels of miR-21. The trend of miR-21 was roughly similar to the changes in the fluorescence intensity of exosomes (Fig. 5J). These results suggest that, through sustained release, GelMA-Ag21Exo enhances the stability and long-term retention of Agomir21-Exo and extend the therapeutic window for miR-21.

3.6. Treatment with GelMA-Ag21Exo reduces GC apoptosis and restores fertility in POI mice

We further assessed the therapeutic efficacy of GelMA-Ag21Exo in VCD-induced POI mice. After weekly injection treatments for three consecutive weeks, we harvested and weighed the ovaries of mice from each group for observation. Compared with those in the NC group, all groups showed various degrees of ovarian atrophy after treatment with VCD. There was no significant improvement in the size or weight of the ovaries in the MSC-Exo group or Agomir21-Exo group relative to the POI group, reflecting the limitations of these treatments, which were inconsistent with the *in vitro* experimental results. However, the size and weight of the ovaries in the GelMA-Ag21Exo group recovered markedly (Fig. 6A and B). A similar trend was observed in the follicle counts based on ovarian H&E-staining. Compared with those in the MSC-Exo group or the Agomir21-Exo group, the number of follicles in the GelMA-Ag21Exo-treated group tended to increase at different stages (Fig. 6C and D). TUNEL staining revealed that the proportion of apoptotic GCs in the GelMA-Ag21Exo group (2.51 ± 0.55 %) was significantly lower than that in the Agomir21-Exo group (5.14 ± 0.90 %), MSC-Exo group (5.71 ± 0.94 %), and POI group (6.18 ± 0.65 %) (Fig. 6E and F).

Subsequently, we assessed the regulatory effect of GelMA-Ag21Exo on the PTEN/Akt pathway in POI mice via Immunohistochemistry. As anticipated, GelMA-Ag21Exo attenuated PTEN expression and augmented p-Akt expression in GCs. Additionally, GelMA-Ag21Exo notably downregulated the expression of cleaved caspase-3 and Bax. Compared to the POI group, the Agomir21-Exo group also showed a similar regulatory trend, although less prominently (Fig. 6G).

We selected three representative mice from each group for estrous cycle analysis. According to the different stages of vaginal epithelial cell morphology (Fig. 6H), we found that mice in the NC group demonstrated stable and regular estrous cycles. Meanwhile, mice of the POI, MSC-Exo, and Agomir21-Exo groups mostly remained in the proestrus and diestrus, while those in the GelMA-Ag21Exo group exhibited a certain recovery in the frequency of estrous (Fig. 6I). Plasma hormone measurements revealed a decrease in the AMH and E2 levels and an increase in the FSH level in the POI group, indicating a decline in ovarian reserve. Compared with those in the MSC-Exo group or the Agomir21-Exo group, the ovarian reserve in the GelMA-Ag21Exo group was better restored, reflected by an increase in AMH and E2 levels and a decrease in FSH levels (Fig. 6J–L).

Following a three-week treatment, six female mice in each group were mated with fertile C57BL/6 male mice. Within three months, all six mice in the NC group successfully conceived and gave birth with the number of pups ranging from 6 to 10. No mice in the POI group conceived successfully. In the MSC-Exo group, two mice conceived, one gave birth to three pups, and the other died due to dystocia. Two mice in the Agomir21-Exo group conceived and gave birth to one and three pups, respectively. All the mice in the GelMA-Ag21Exo group successfully conceived, although one gave birth to a stillborn foetus (Fig. 6M–O). These results suggested that treatment with GelMA-Ag21Exo inhibited VCD-induced GC apoptosis and partially restored the ovarian reserve and fertility.

4. Discussion

The restoration of ovarian function and the achievement of pregnancy in patients with POI are long-standing challenges. In recent years, Assisted Reproductive Technologies (ART) has made significant contributions to enhancing pregnancy outcomes among infertile patients. However, even with ART assistance, women with POI still struggle to conceive. MSC-Exo has been demonstrated to be a potential therapy for POI and it has been reported that intravenous injections of MSC-Exo can restore ovarian function and consequently facilitate pregnancy in POI mouse models [39]. Moreover, some scholars believe that the stimulating effect of MSC-Exo on primordial follicles is achieved through the

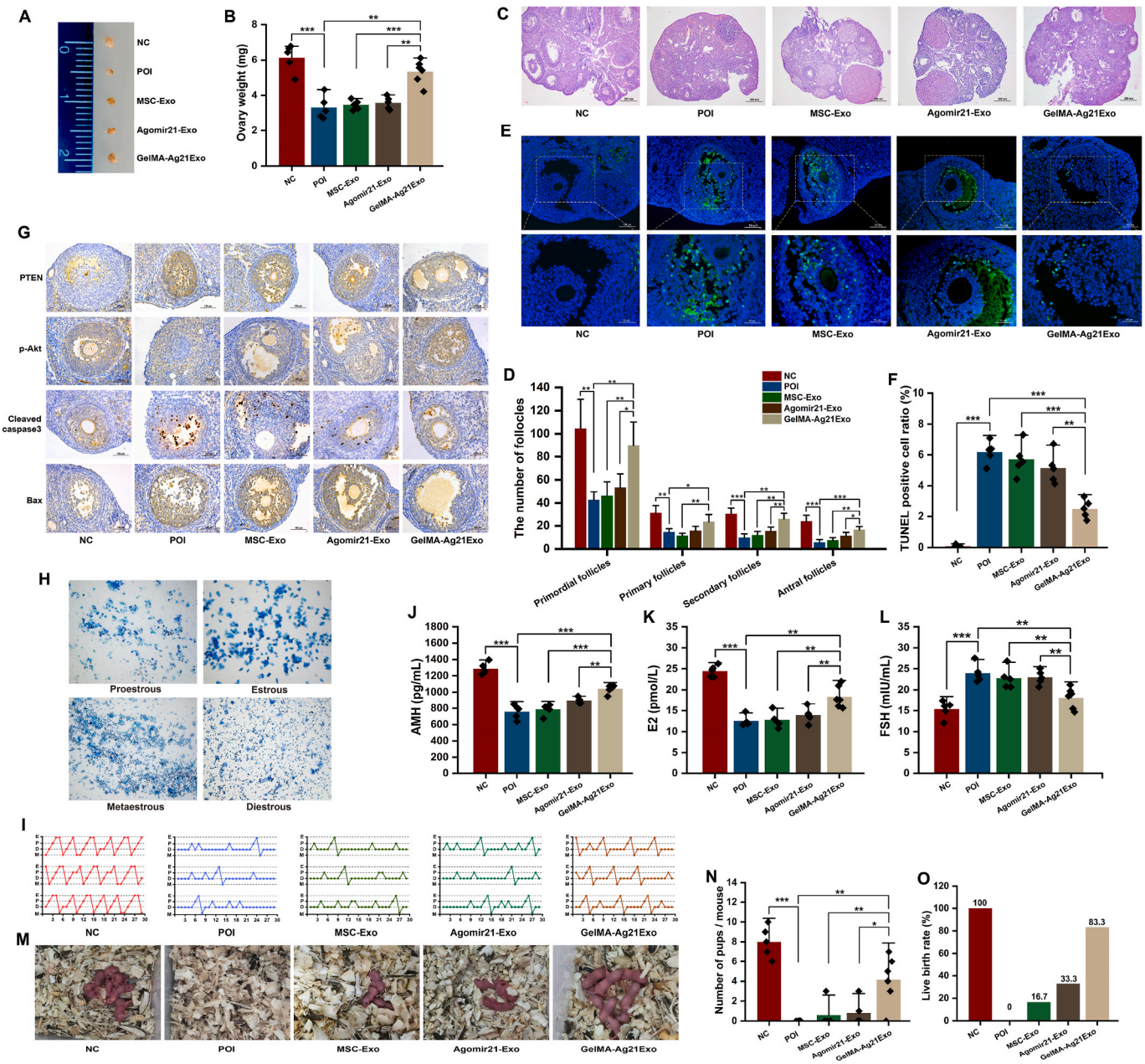

Fig. 6. Therapeutic effect of GelMA-Ag21Exo**.** (A) The size of the ovaries in different groups, including the NC group, POI group, MSC-Exo group, Agomir21-Exo group, and GelMA-Ag21Exo group. (B) Statistical analyses of ovary weight in all groups. (C, D) H&E staining of the ovaries and follicle counts at each stage. (E) TUNEL staining (GREEN) of the ovaries in each group representing apoptotic GCs and DAPI staining (BLUE) representing all cell nuclei. (F) Statistical analyses of TUNEL positive cells across all groups. (G) Immunohistochemistry of PTEN, p-Akt, cleaved caspase-3, and Bax in GCs of the ovaries across all groups. (H) Vaginal epithelial cell morphology at different stages of the estrous cycle. (I) Estrous cycle of mice in all groups. (J–K) Results of ELISA tests measuring levels of AMH, E2, and FSH in mouse serum across all groups. (M, N) The results of the fertility test. The number of offspring of NC group, POI group, MSC-Exo group, Agomir21-Exo group, and GelMA-Ag21Exo group were 48, 0, 3, 4, and 25, respectively. (O) The live birth rates of the five groups were 100 %, 0 %, 16.7 %, 33.3 % and 83.3 %, respectively.

Notes: The data are presented as mean ± standard deviation (SD) from at least three independent experiments. *P < 0.05, **P < 0.01, ***P < 0.001.

transport of miR-21 [40]. miR-21, one of the most extensively studied miRNAs, has been proven to inhibit the apoptosis of rat GCs [34]. According to our study, miR-21 is one of the most abundant miRNAs found in human FF-Exo, and its expression is notably reduced in POI-FF-Exo. And the lack of miR-21 in GCs can lead to overexpression of PTEN, resulting in growth retardation and cell apoptosis. However, supplementing exogenous miR-21 can inhibit the PTEN/Akt pathway, restore cell viability, and suppress GC apoptosis. This suggested that replenishing the lack of miR-21 might be a natural and efficient remedy for the apoptosis of GCs in POI patients.

We loaded exogenetic Agomir-21 into MSC-Exo, which formed a small molecule drug with strong anti-apoptotic effect, Agomir21-Exo. However, the *in vivo* application of exosomes is restricted due to their short half-life, resulting in unsatisfactory therapeutic effects. One study suggested that more than half of the exosomes present in the circulatory system are cleared 60 min after intravenous injection and are almost completely exhausted after 180 min [41]. Another report indicated that the majority of exosomes in the blood are cleared 10–15 min post injection and are nearly undetectable after 24 h. Furthermore, in the organs of mice, the exosome signal gradually increases within 1–4 h and

significantly decreases after 24 h [42]. These findings suggest that the short duration of action of the exosomes may lead to reduced therapeutic efficacy *in vivo* [39]. Hence, we developed GelMA-Ag21Exo microspheres to achieve the controllable sustained release of Agomir21-Exo *in vivo* based on the characteristics of GelMA hydrogel. Depending on the properties of the added DMPC, the microspheres showed excellent injectability. According to our studies, 15 % GelMA-Ag21Exo microspheres prolong the therapeutic window of Agomir21-Exo treatment to more than 7 days, resulting in a significant improvement in therapeutic effects in mice with POI.

Constrained by current technical limitations, we are unable to precisely monitor the release kinetics of Agomir21-Exo from GelMA microspheres, introducing uncertainties in the *in vivo* application of GelMA-Ag21Exo. In the fertility test, the limited number of offspring produced after VCD treatment raises concerns about the reliability of certain data. Ideally, additional breeding experiments with mice should be conducted under controlled conditions, continuously tracking changes in body weight and fertility of the offspring to better elucidate the therapeutic efficacy of GelMA-Ag21Exo proposed in this study. Despite the ability of GelMA-Ag21Exo to facilitate the sustained release of Agomir21-Exo and enhance its therapeutic efficacy, the lack of specificity could potentially result in the waste of the majority of Agomir21-Exo during transport. Researches indicate that exosomes injected into the mouse circulatory system are primarily distributed in organs that possess the MPS, such as the liver, spleen, and lungs [41,43,44]. It is foreseeable that only a small portion of exosomes can be taken up by the ovaries. To address these challenges, the engineering of exosomes could be an effective approach. Specifically, exosomes decorated with certain targeting molecules could achieve more precise therapeutic cargo delivery [45,46]. The combination of engineered exosomes and injectable hydrogel microspheres could further optimize the therapeutic effect of Agomir-21, which is worthy of further investigation.

5. Conclusion

Overall, in the present study, we devised GelMA-Ag21Exo microspheres based on GelMA hydrogel, which facilitated the controlled and sustained release of Agomir21-Exo in mice. Through the inhibitory effect of miR-21 on GC apoptosis via the PTEN/Akt pathway, GelMA-Ag21Exo notably improved the ovarian reserve and fertility of POI mice. In a word, our study provides a simplistic and effective therapy for POI.

CRediT authorship contribution statement

Xiaofei Zhang: Writing – original draft, Visualization, Methodology, Data curation. **Linzi Ma:** Writing – review & editing, Resources, Methodology. **Xiaotong Liu:** Validation, Formal analysis. **Xingyu Zhou:** Supervision, Project administration. **Ao Wang:** Validation, Methodology. **Yunhui Lai:** Validation, Methodology. **Jun Zhang:** Investigation. **Ying Li:** Methodology. **Shiling Chen:** Writing – review & editing, Resources, Project administration, Funding acquisition, Conceptualization.

Disclosure

The authors declare that there are no conflicts of interest associated with this work.

Ethics approval and consent to participate

The study of human granulosa cell samples was approved by the Ethics Committee of Nanfang Hospital, Southern Medical University (NFEC-2017–197), and was carried out in accordance with the Declaration of Helsinki. Written informed consent was obtained from all patients. All animal procedures were approved by the Animal Use and Care Ethics Committee of Nanfang Hospital, Southern Medical University, and were complied with the National Institutes of Health Guide for the Care and Use of Laboratory Animals.

Funding

This work was supported by the National Natural Science Foundation of China (81901559), the Guangdong Basic and Applied Basic Research Foundation (2021A1515011061), the Clinical Research Program of Nanfang Hospital, Southern Medical University (2018CR016).

Declaration of competing interest

The authors declare that they have no known competing financial interests or personal relationships that could have appeared to influence the work reported in this paper.

Acknowledgments

We gratefully acknowledge all the staff of the Center for Reproductive Medicine, Department of Gynecology and Obstetrics, Nanfang Hospital, Southern Medical University for their support and cooperation.

Appendix A. Supplementary data

Supplementary data to this article can be found online at https://doi.org/10.1016/j.mtbio.2025.101469.

Data availability

Data will be made available on request.

References

[1] L. Webber, M. Davies, R. Anderson, J. Bartlett, D. Braat, B. Cartwright, R. Cifkova, K.S. de Muinck, E. Hogervorst, F. Janse, L. Liao, V. Vlaisavljevic, C. Zillikens, N. Vermeulen, Hum. Reprod. 31 (5) (2016) 926–937, https://doi.org/10.1093/humrep/dew027.
[2] L.R. Schover, J. Clin. Oncol. 26 (5) (2008) 753–758, https://doi.org/10.1200/JCO.2007.14.1655.
[3] G.D. Mishra, M.C. Davies, S. Hillman, H.F. Chung, S. Roy, K. Maclaran, M. Hickey, Lancet 403 (10430) (2024) 958–968, https://doi.org/10.1016/S0140-6736(23)02800-3.
[4] C.K. Yeung, G. Wang, Y. Yao, J. Liang, C.C. Tenny, M. Chuai, K.K. Lee, X. Yang, Cell Death Dis. 8 (3) (2017) e2697, https://doi.org/10.1038/cddis.2017.91.
[5] X. Wang, X. Zhang, Y. Dang, D. Li, G. Lu, W.Y. Chan, P. Leung, S. Zhao, Y. Qin, Z. J. Chen, Nucleic Acids Res. 48 (8) (2020) 4480–4491, https://doi.org/10.1093/nar/gkaa127.
[6] R. Machtinger, L.C. Laurent, A.A. Baccarelli, Hum. Reprod. Update 22 (2) (2016) 182–193, https://doi.org/10.1093/humupd/dmv055.
[7] Q. Zhou, Z. Liu, Z. Liao, Y. Zhang, M. Qu, F. Wu, J. Tian, H. Zhao, Q. Peng, W. Zheng, M. Huang, S. Yang, J. Cell. Physiol. 239 (1) (2024) 20–35, https://doi.org/10.1002/jcp.31140.
[8] C. Chen, Z. Zhang, X. Gu, X. Sheng, L. Xiao, X. Wang, Mater. Today Bio 19 (2023) 100608, https://doi.org/10.1016/j.mtbio.2023.100608.
[9] S. Zhang, B.H. Yahaya, Y. Pan, Y. Liu, J. Lin, Stem Cell Res. Ther. 14 (1) (2023) 327, https://doi.org/10.1186/s13287-023-03551-w.
[10] S. Zhang, D. Zhu, X. Mei, Z. Li, J. Li, M. Xie, H. Xie, S. Wang, K. Cheng, Bioact. Mater. 6 (7) (2021) 1957–1972, https://doi.org/10.1016/j.bioactmat.2020.12.008.
[11] C. Akyurekli, Y. Le, R.B. Richardson, D. Fergusson, J. Tay, D.S. Allan, Stem Cell Rev. Rep. 11 (1) (2015) 150–160, https://doi.org/10.1007/s12015-014-9545-9.
[12] S. Keshtkar, N. Azarpira, M.H. Ghahremani, Stem Cell Res. Ther. 9 (1) (2018) 63, https://doi.org/10.1186/s13287-018-0791-7.
[13] B. Huang, J. Lu, C. Ding, Q. Zou, W. Wang, H. Li, Stem Cell Res. Ther. 9 (1) (2018) 216, https://doi.org/10.1186/s13287-018-0953-7.
[14] L.P. Zhu, T. Tian, J.Y. Wang, J.N. He, T. Chen, M. Pan, L. Xu, H.X. Zhang, X.T. Qiu, C.C. Li, K.K. Wang, H. Shen, G.G. Zhang, Y.P. Bai, Theranostics 8 (22) (2018) 6163–6177, https://doi.org/10.7150/thno.28021.
[15] E. Oveili, S. Vafaei, H. Bazavar, Y. Eslami, E. Mamaghanizadeh, S. Yasamineh, O. Gholizadeh, Cell Commun. Signal. 21 (1) (2023) 20, https://doi.org/10.1186/s12964-022-01017-9.
[16] D.C. Watson, D. Bayik, A. Srivatsan, C. Bergamaschi, A. Valentin, G. Niu, J. Bear, M. Monninger, M. Sun, A. Morales-Kastresana, J.C. Jones, B.K. Felber, X. Chen, I. Gursel, G.N. Pavlakis, Biomaterials 105 (2016) 195–205, https://doi.org/10.1016/j.biomaterials.2016.07.003.

[17] K.W. Witwer, E.I. Buzás, L.T. Bemis, A. Bora, C. Lässer, J. Lötvall, H.E. Nolte-'T, M. G. Piper, S. Sivaraman, J. Skog, C. Théry, M.H. Wauben, F. Hochberg, J. Extracell. Vesicles 2 (2013), https://doi.org/10.3402/jev.v2i0.20360.
[18] R. Zhong, S. Talebian, B.B. Mendes, G. Wallace, R. Langer, J. Conde, J. Shi, Nat. Mater. 22 (7) (2023) 818–831, https://doi.org/10.1038/s41563-023-01472-w.
[19] S.E. Appt, J.R. Kaplan, T.B. Clarkson, J.M. Cline, P.J. Christian, P.B. Hoyer, Fertil. Steril. 86 (4 Suppl) (2006) 1210–1216, https://doi.org/10.1016/j.fertnstert.2006.05.004.
[20] Y. Han, J. Yang, W. Zhao, H. Wang, Y. Sun, Y. Chen, J. Luo, L. Deng, X. Xu, W. Cui, H. Zhang, Bioact. Mater. 6 (10) (2021) 3596–3607, https://doi.org/10.1016/j.bioactmat.2021.03.022.
[21] J. Bian, F. Cai, H. Chen, Z. Tang, K. Xi, J. Tang, L. Wu, Y. Xu, L. Deng, Y. Gu, W. Cui, L. Chen, Nano Lett. 21 (6) (2021) 2690–2698, https://doi.org/10.1021/acs.nanolett.0c04713.
[22] J. Liu, Z. Zhou, M. Hou, X. Xia, Y. Liu, Z. Zhao, Y. Wu, Y. Deng, Y. Zhang, F. He, Y. Xu, X. Zhu, Mater. Today Bio 25 (2024) 100956, https://doi.org/10.1016/j.mtbio.2024.100956.
[23] K. Yue, S.G. Trujillo-de, M.M. Alvarez, A. Tamayol, N. Annabi, A. Khademhosseini, Biomaterials 73 (2015) 254–271, https://doi.org/10.1016/j.biomaterials.2015.08.045.
[24] J.W. Nichol, S.T. Koshy, H. Bae, C.M. Hwang, S. Yamanlar, A. Khademhosseini, Biomaterials 31 (21) (2010) 5536–5544, https://doi.org/10.1016/j.biomaterials.2010.03.064.
[25] W. Lin, M. Kluzek, N. Iuster, E. Shimoni, N. Kampf, R. Goldberg, J. Klein, Science 370 (6514) (2020) 335–338, https://doi.org/10.1126/science.aay8276.
[26] A.P. Ferraretti, A. La Marca, B.C. Fauser, B. Tarlatzis, G. Nargund, L. Gianaroli, Hum. Reprod. 26 (7) (2011) 1616–1624, https://doi.org/10.1093/humrep/der092.
[27] X.Y. Zhou, Y. Li, J. Zhang, Y.D. Liu, J. Zhe, Q.Y. Zhang, Y.X. Chen, X. Chen, S. L. Chen, Epigenomics 12 (4) (2020) 319–332, https://doi.org/10.2217/epi-2019-0147.
[28] L.B. Cao, C.K. Leung, P.W. Law, Y. Lv, C.H. Ng, H.B. Liu, G. Lu, J.L. Ma, W.Y. Chan, Life Sci. 262 (2020) 118543, https://doi.org/10.1016/j.lfs.2020.118543.
[29] H. Xu, Y. Xia, J. Qin, J. Xu, C. Li, Y. Wang, Reprod. Biol. Endocrinol. 19 (1) (2021) 113, https://doi.org/10.1186/s12958-021-00799-w.
[30] L. Kalich-Philosoph, H. Roness, A. Carmely, M. Fishel-Bartal, H. Ligumsky, S. Paglin, I. Wolf, H. Kanety, B. Sredni, D. Meirow, Sci. Transl. Med. 5 (185) (2013) 185ra62, https://doi.org/10.1126/scitranslmed.3005402.
[31] C. Théry, L. Zitvogel, S. Amigorena, Nat. Rev. Immunol. 2 (8) (2002) 569–579, https://doi.org/10.1038/nri855.
[32] K. Zhai, H. Duan, W. Wang, S. Zhao, G.J. Khan, M. Wang, Y. Zhang, K. Thakur, X. Fang, C. Wu, J. Xiao, Z. Wei, Acta Pharm. Sin. B 11 (11) (2021) 3493–3507, https://doi.org/10.1016/j.apsb.2021.03.032.
[33] F. Olivieri, F. Prattichizzo, A. Giuliani, G. Matacchione, M.R. Rippo, J. Sabbatinelli, M. Bonafè, Ageing Res. Rev. 70 (2021) 101374, https://doi.org/10.1016/j.arr.2021.101374.
[34] X. Fu, Y. He, X. Wang, D. Peng, X. Chen, X. Li, Q. Wang, Stem Cell Res. Ther. 8 (1) (2017) 187, https://doi.org/10.1186/s13287-017-0641-z.
[35] A.J. Hsueh, K. Kawamura, Y. Cheng, B.C. Fauser, Endocr. Rev. 36 (1) (2015) 1–24, https://doi.org/10.1210/er.2014-1020.
[36] M. Kou, L. Huang, J. Yang, Z. Chiang, S. Chen, J. Liu, L. Guo, X. Zhang, X. Zhou, X. Xu, X. Yan, Y. Wang, J. Zhang, A. Xu, H.F. Tse, Q. Lian, Cell Death Dis. 13 (7) (2022) 580, https://doi.org/10.1038/s41419-022-05034-x.
[37] S. Ramanathan, B.B. Shenoda, Z. Lin, G.M. Alexander, A. Huppert, A. Sacan, S. K. Ajit, J. Extracell. Vesicles 8 (1) (2019) 1650595, https://doi.org/10.1080/20013078.2019.1650595.
[38] J. Tian, Z. Han, D. Song, Y. Peng, M. Xiong, Z. Chen, S. Duan, L. Zhang, Int. J. Nanomed. 18 (2023) 7923–7940, https://doi.org/10.2147/IJN.S444582.
[39] H.S. Park, R.M. Chugh, J. Seok, E. Cetin, H. Mohammed, H. Siblini, A.F. Liakath, M. M. Ghasroldasht, H. Alkelani, A. Elsharoud, M. Ulin, S. Esfandyari, A. Al-Hendy, Stem Cell Res. Ther. 14 (1) (2023) 165, https://doi.org/10.1186/s13287-023-03397-2.
[40] W. Yang, J. Zhang, B. Xu, Y. He, W. Liu, J. Li, S. Zhang, X. Lin, D. Su, T. Wu, J. Li, Mol. Ther. 28 (4) (2020) 1200–1213, https://doi.org/10.1016/j.ymthe.2020.02.003.
[41] C.P. Lai, O. Mardini, M. Ericsson, S. Prabhakar, C. Maguire, J.W. Chen, B. A. Tannous, X.O. Breakefield, ACS Nano 8 (1) (2014) 483–494, https://doi.org/10.1021/nn404945r.
[42] E. Lázaro-Ibáñez, F.N. Faruqu, A.F. Saleh, A.M. Silva, W.J. Tzu-Wen, J. Rak, K. T. Al-Jamal, N. Dekker, ACS Nano 15 (2) (2021) 3212–3227, https://doi.org/10.1021/acsnano.0c09873.
[43] D.H. Kim, V.K. Kothandan, H.W. Kim, K.S. Kim, J.Y. Kim, H.J. Cho, Y.K. Lee, D. E. Lee, S.R. Hwang, Pharmaceutics 11 (12) (2019), https://doi.org/10.3390/pharmaceutics11120649.
[44] X. Zhang, H. Zhang, J. Gu, J. Zhang, H. Shi, H. Qian, D. Wang, W. Xu, J. Pan, H. A. Santos, Adv. Mater. 33 (14) (2021) e2005709, https://doi.org/10.1002/adma.202005709.
[45] M. Zhang, S. Hu, L. Liu, P. Dang, Y. Liu, Z. Sun, B. Qiao, C. Wang, Signal Transduct. Target. Ther. 8 (1) (2023) 124, https://doi.org/10.1038/s41392-023-01382-y.
[46] Y. Yang, Y. Hong, E. Cho, G.B. Kim, I.S. Kim, J. Extracell. Vesicles 7 (1) (2018) 1440131, https://doi.org/10.1080/20013078.2018.1440131.